Numerical Modelling of Duplex Stainless Steel Structures

Priscila das N. Pereira; William M. Pereira; Isabella Pinheiro Gueiros, Luciano Rodrigues Ornelas de Lima, Pedro Colmar Gonçalves da Silva Vellasco, José Guilherme Santos da Silva

Structural Engineering Department, UERJ, Brazil

ABSTRACT

Current stainless steel design codes like the Eurocode 3, part 1.4, are still largely based in carbon steel structural analogies. This strategy was used as a first attempt to produce specific stainless steel structural design rules, enabling engineers to perform a smooth transition for the stainless steel design. The present paper presents an investigation aiming to evaluate the lateral buckling capacity of duplex stainless steel beams and the resistance of tubular T joints between RHS members constituted by duplex stainless steel. The results are discussed and compared in terms of the stress distribution, force-displacement curves, etc. An assessment of the results against the Eurocode 3 pt. 1.4 provisions is also presented.

1 Introduction

Stainless steel have been used in various types of constructions due to its main characteristics associated to high corrosion resistance, durability, fire resistance [1], ease of maintenance, appearance and aesthetics. The development of the construction process and, the new tendencies adopted in the architecture design conception, highlighted the need for materials that can combine versatility with durability. Stainless steel is indicated, as a structural element in construction for multiple reasons. Its high ductility allows its use in structures subjected to cyclic loadings, through load redistributions before the structural collapse. The cost reduction achieved with the less need for structure maintenance, and the increase in its capacity to dissipate impact loads, also enhanced the stainless steel structure reliability.

Changes of attitudes associated to the building construction industry and a global transition for a sustainability development reduction in environmental impacts has been causing an increase in the stainless steel use as it can be observed in the Figure 1. Despite these facts, Current stainless steel design codes like the Eurocode 3, part 1.4 [2], are still largely based in carbon steel structural analogies [3]. This strategy was used as a first attempt to produce specific stainless steel structural design rules, enabling engineers to perform a smooth transition for the stainless steel design.

a) Arco de Malizia, Italy b) Piove di Sacco, Italy

Figure 1 – Examples of stainless steel structures

The present paper presents an investigation aiming to evaluate the lateral buckling capacity of duplex stainless steel beams and the resistance of tubular T joints between RHS members constituted by duplex stainless steel. The results are discussed and compared in terms of the stress distribution, force-displacement curves, etc. An assessment of the results with the Eurocode 3 pt. 1.4 [2] provisions is also presented.

2 Design Codes Recommendations

2.1 Lateral Torsional Buckling Resistance

According to Eurocode 3 part 1.4 [2], the elastic critical moment can be estimated using expression (1), proposed by Clark and Hill (1960) and Galéa (1981) and reported by Silva et al. [4]. This is applicable to members subject to bending about the strong axis, with cross sections mono-symmetric about the weak *z* axis, for several support conditions and types of loading.

$$M_{cr} = C_1 \frac{\pi^2 E I_z}{(k_z L)^2} \left\{ \left[\left(\frac{k_z}{k_w} \right)^2 \frac{I_W}{I_z} + \frac{(k_z L)^2 G I_T}{\pi^2 E I_z} + (C_2 z_g - C_3 z_j)^2 \right]^{0.5} - (C_2 z_g - C_3 z_j) \right\} \quad (1)$$

where,

- C_1, C_2 and C_3 are coefficients depending on the bending moment diagram and on support conditions, given in Table 1 for the case investigated in this paper;
- k_z and k_w are effective length factors that depend on the support conditions at the end sections. Factor k_z is related to rotations at the end sections about the weak axis *z*, and k_w refers to warping restriction in the same cross sections. These factors vary between 0.5 (restrained deformations) and 1.0 (free deformations), and are equal to 0.7 in the case of free deformations at one end and restrained at the other. Since in most practical situations restraint is only partial, conservatively a value of $k_z = k_w = 1.0$ may be adopted;
- $z_g = (z_a - z_s)$, where z_a and z_s are the coordinates of the load application point and shear centre, relative to the cross section centroid; these quantities are positive if located in the part of the cross section under compression and negative if located in the part of the cross section under tension;
- $z_j = z_s - \left(0.5 \int_A (y^2 + z^2)(z/I_y) dA \right)$ is a parameter that reflects the degree of asymmetry of the cross section in relation to the *y* axis. It is zero for beams with doubly symmetric cross section (such as I or H cross sections with equal flanges) and adopts positive values when the flange with the largest second moment of area about *z* is the flange under compress, at the cross section with the maximum bending moment;

Table 1 Coefficients C1, C2 and C3 for simply supported beams with a central concentrated load

Loading and support conditions	Diagram of moments	kz	C_1	C_2	C_3
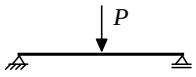	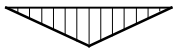	1.0	1.35	0.59	0.411
		0.5	1.05	0.48	0.338

Due to the presence of geometrical imperfections, the actual behaviour of a member diverges from the theoretical behaviour and the elastic critical moment is never reached. Eurocode 3, part 1.4 [2], in order to evaluate the resistance to lateral-torsional buckling of a prismatic member prescribes the verification of the following condition:

$$\frac{M_{Ed}}{M_{b,Rd}} \leq 1.0 \quad (2)$$

where M_{Ed} is the bending moment design value and $M_{b,Rd}$ is the design buckling resistance, given by

$$M_{b,Rd} = \chi_{LT} W_y f_y / \gamma_{M1} \quad (3)$$

where $W_y = W_{pl,y}$ for class 1 and 2 cross sections and χ_{LT} is the reduction factor for lateral-torsional buckling.

In Eurocode 3, part 1.4 [2], two methods for the evaluation of the reduction coefficient χ_{LT} in prismatic members are proposed: a general method that can be applied to any type of cross section (more conservative) and an alternative method that can be applied to rolled cross sections or equivalent welded sections. In this work, the general method will be used. In this method, the reduction factor χ_{LT} is determined by the following expression:

$$\chi_{LT} = \frac{1}{\phi_{LT} + \left(\phi_{LT}^2 - \overline{\lambda}_{LT}^2 \right)^{0.5}}, \quad \text{but } \chi_{LT} \leq 1.0, \quad (4)$$

with: $\phi_{LT} = 0.5\left[1 + \alpha_{LT}\left(\overline{\lambda}_{LT} - 0.2\right) + \overline{\lambda}_{LT}^2\right]$;

α_{LT} is the imperfection factor, which depends on the buckling curve;

$\overline{\lambda}_{LT} = \left[W_y f_y / M_{cr}\right]^{0.5}$;

M_{cr} the elastic critical moment.

The buckling curves to be adopted depend on the geometry of the cross section of the member. For I or H rolled sections, curve a is used if $h/b \le 2$ and curve b is used if $h/b > 2$. For I or H welded sections, curve c is used if $h/b \le 2$ and curve d is used is used if $h/b > 2$. For the imperfection factors α_{LT} associated to the various curves, the values are 0.13, 0.21, 0.34, 0.49 and 0.76 for curves a_0, a, b, c and d (European design buckling curves), respectively.

2.2 RHS Tubular Joint Resistance

2.2.1 Eurocode 3 and CIDECT formulations

Some of the most common types of connections using hollow sections are: “T”, “K”, “KT” and “Y” joints. This study was focused on the behaviour of fully welded connections between square hollow sections (SHS) performing a “T-joint”. Figure 2 shows the geometry of these connections and the main geometrical parameters. The main member (horizontal in this case) is the chord and the secondary member (vertical in this example) is the brace.

According to Eurocode 3 part 1.1 [3] and CIDECT [4], some geometrical limits need to be verified prior to the evaluation of the joint resistance. These limits are also presented in Figure 2 where b and t represent, respectively, the tube width and thickness.

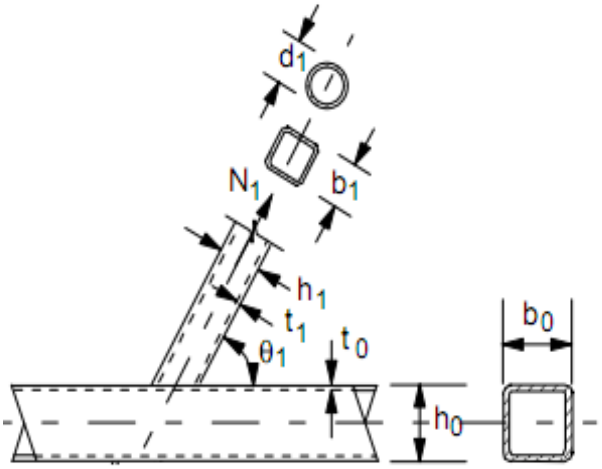

$$0{,}25 \le \beta = b_i / b_0 \le 0{,}85 \quad \text{(EC3)} \quad (5)$$

$$0{,}25 \le \beta = b_i / b_0 \le 0{,}80 \quad \text{(CIDECT)} \quad (6)$$

$$b_i / b_0 \ge 0{,}1 + 0{,}01 b_0 / t_0 \quad \text{(CIDECT)} \quad (7)$$

$$2\gamma = b_i / t_i \le 50 \quad \text{(CIDECT)} \quad (8)$$

$$0{,}5 \le h_o / b_o \le 2{,}0 \quad \text{(EC3)} \quad (9)$$

$$0{,}5 \le h_i / b_i \le 2{,}0 \quad \text{(EC3)} \quad (10)$$

$$2\gamma = h_0 / t_0 \le 40 \quad \text{(CIDECT)} \quad (11)$$

$$2\gamma = b_0 / t_0 \le 40 \quad \text{(CIDECT)} \quad (12)$$

$$b_0 / t_0 \le 35 \quad \text{(EC3)} \quad (13)$$

$$b_i / t_i \le 35 \quad \text{(EC3)} \quad (14)$$

The failure modes considered by the Eurocode 3, part 1.8 [3] are presented in Figure 2. The failure modes considered by the EC3 for the “T-joints” under axial load are the modes a, b, d, e and f. This approach is valid for cases with $\beta \ge 0.25$, $\mu_0 \le 35$ and $\mu_1 \le 35$, respectively. All the evaluated joints had the b parameter smaller than 0.85, so only the chord face failure ultimate limit state should be considered. For this ultimate limit state, the joints resistance according to Eurocode 3 is given by the follow equation:

$$N_{1,Rd} = \frac{k_n . f_{y0} . t_0^2}{(1-\beta) . \text{sen}\theta_1}\left(\frac{2.\eta}{\text{sen}\theta_1} + 4.\sqrt{1-\beta}\right) / \gamma_{M5} \quad (15)$$

where $N_{1,Rd}$ is the chord face failure resistance,

k_p is taken equal to 1.0 for tension brace loads,

f_{y0} is the chord yield stress,

β is a geometrical parameter according to *Eq.* (5),

γ_{M5} is the partial safety factor, in this case equal to 1.

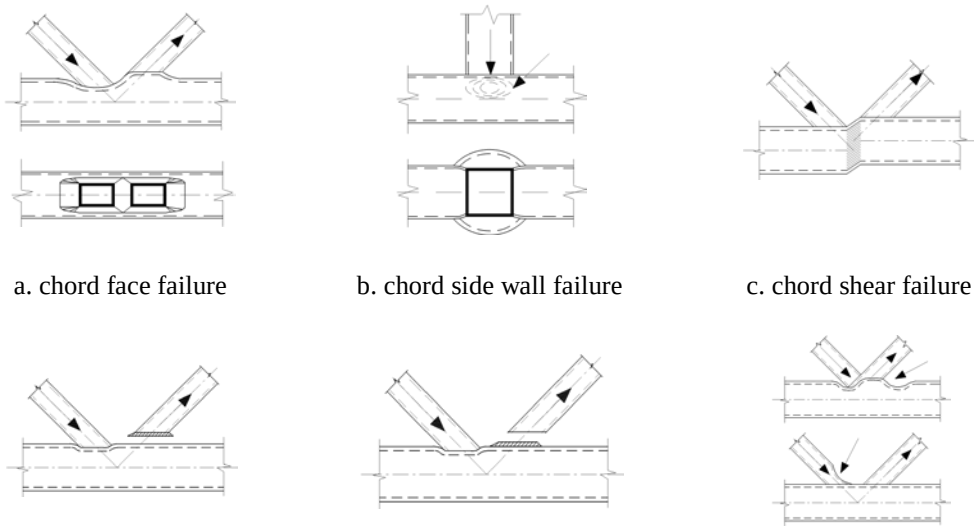

a. chord face failure b. chord side wall failure c. chord shear failure

d. punching shear e. brace failure f. local buckling

Figure 2 – Examples of stainless steel structures

The new joint strength *Eq.* (5) for chord plastification according to CIDECT [4] are expressed in terms of Q_u (influence of the parameters β and γ) and Q_f (influence of the parameter n). In these equations, the parameter C_1 is taken equal to 0.5-0.5β ($C_1 \geq 0.10$) for chord compression stresses ($n<0$) and equal to 1.0 for chord tension stresses ($n \geq 0$). For the distinction with the formulae present in the previous edition, which are incorporated in various national and international codes, a slightly different presentation is used and described below.

$$N_1^* = Q_u.Q_f.\frac{f_{y0}.t_0^2}{\text{sen}\theta_i} \quad \text{com} \quad Q_u = \frac{2.\eta}{(1-\beta)\text{sen}\theta_i} + \frac{4}{\sqrt{1-\beta}} \quad \text{e} \quad Q_f = (1-|n|)^{C_1} \tag{16}$$

$$n = \frac{N_0}{N_{pl,0}} + \frac{M_0}{M_{pl,0}} \tag{17}$$

2.2.2 Feng and Young Formulation [10]

Feng and Young [10] conducted a series of tests on cold-formed stainless steel SHS and RHS T- and X-joints using duplex stainless steel (EN 1.4462). According Feng and Young [10] studies, chord face failure occurred when the brace width to chord width ratio $\beta < 0.7$. The existing design formulae in the current CIDECT [4] and Eurocode [7] for carbon steel tubular T- and X-joints failed at the chord face were developed based on the yield line theory. In this study, a reduction factor (αA) is introduced and the term f(n) in the current CIDECT [4] and Eurocode [3] that accounts for the influence of chord preload is modified to predict the joint strengths of cold formed stainless steel tubular T- and X-joints. Thus, the proposed design equation to predict the nominal strength (N_{1np}) for chord face failure is:

$$N_{1np} = \alpha_A.N_1.1{,}1 \tag{18}$$

where N_{1np} is the proposed nominal strength for chord face failure, and N_1 is the design strength obtained from the current CIDECT [4] and Eurocode [3] for chord face failure given by equation (15) multiplied by f(n). In this work, since the compressive chord preload was not applied, f(n) was taken equal to 1.0. The a_A parameter is obtained from equation (19).

$$\alpha_A = 1 - \frac{b_0}{100t_0} \tag{19}$$

3 Deformation Limit Criteria

Usually, the steel tubular joints design rules are based on plastic analysis or in deformation limits criteria [12], [19]. In a plastic analysis using the yield lines method, each kinetically allowable failure mechanism is associated to a structural load multiplier that is greater or equal to its failure multiplier. The solution however depends on the adopted mechanism. Some examples may be cited [7], [12], [17], [18]. The deformation limits criteria usually associated to the out of

plane loaded chord face ultimate limit state that corresponds to the maximum deformation of this component in this particular direction.

The reason for using deformation limit criteria is that, for slender chord faces, the joint stiffness does not vanish after the full yield and may reach elevated values due to membrane effects. This phenomenon can be observed experimentally and in the curves obtained from numerical simulations incorporating the geometrical and physical nonlinearities and will be discussed later in detail. It is evident that a greater maximum load is reached in experimental tests, but the absence of the knee in these curves may difficult the identification of the point corresponding to the ultimate limit state. Consequently, an alternative to enable comparisons of experimental results to results obtained from plastic analysis is usually based on deformation limit criteria.

The deformation limit proposed by Lu *et al.* [14], [15] and cited by Choo *et al*. [8] may be used in the axial or bending loads evaluation for joints subjected to bending and axial internal forces. The joint resistance is based on the comparison of the deformation in the intersection chord-brace for two loads levels: the ultimate resistance, N_u, that corresponds to a chord out of plane displacement of $\Delta_u = 0.03d_0$, and the serviceability limit, N_s, obtained from a out of plane displacement $\Delta_s = 0.01d_0$ according to Figure 4.

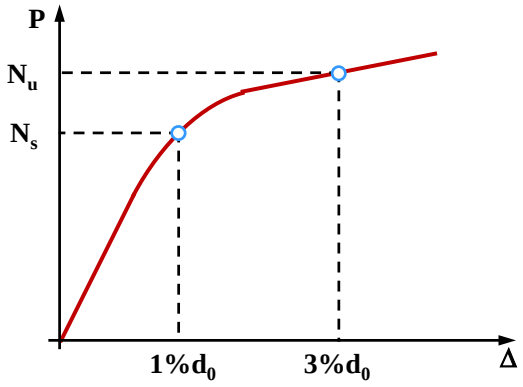

Figure 3 – Examples of stainless steel structures

4 Numerical Modelling

These numerical model were developed in the Ansys 12.0 FEM package [6] using shell elements - SHELL181 – with six degrees of freedom per node, i.e., translations and rotations about X, Y and Z axis. This model is presented in Figure 4, where it can be noticed that the mesh was more refined near the welds and more regular and coarse in the remaining parts to avoid numerical convergence problems. A Newton Raphson algorithm was considered in the Ansys 12.0 FEM package [6] to obtain the nonlinear solution. The load control was based on equivalent displacements. The physical nonlinearity was considered through the von Mises yield criteria and the geometrical nonlinearity was evaluated using Updated Lagrangian Formulation. A multi linear material constitutive law for duplex stainless steel was considered. For the RHS tubular joint, this one was based on Feng and Young [10] tensile coupon tests. This material property is summarized on Table 1. For the duplex stainless steel beam, a standard curve was used. In this model, an initial imperfection corresponding to the maximum value allowed in Eurocode 3 was considered obtained from an eigenvalue analysis analysis based on the first buckling mode.

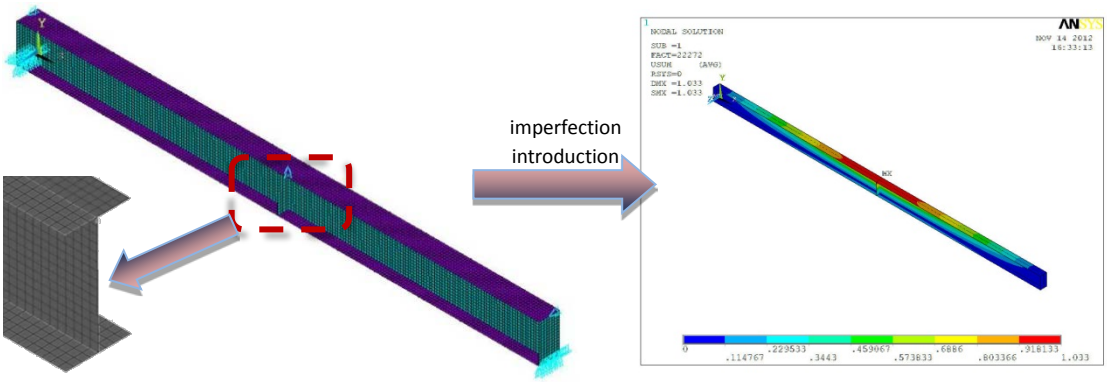

a) duplex stainless steel beams

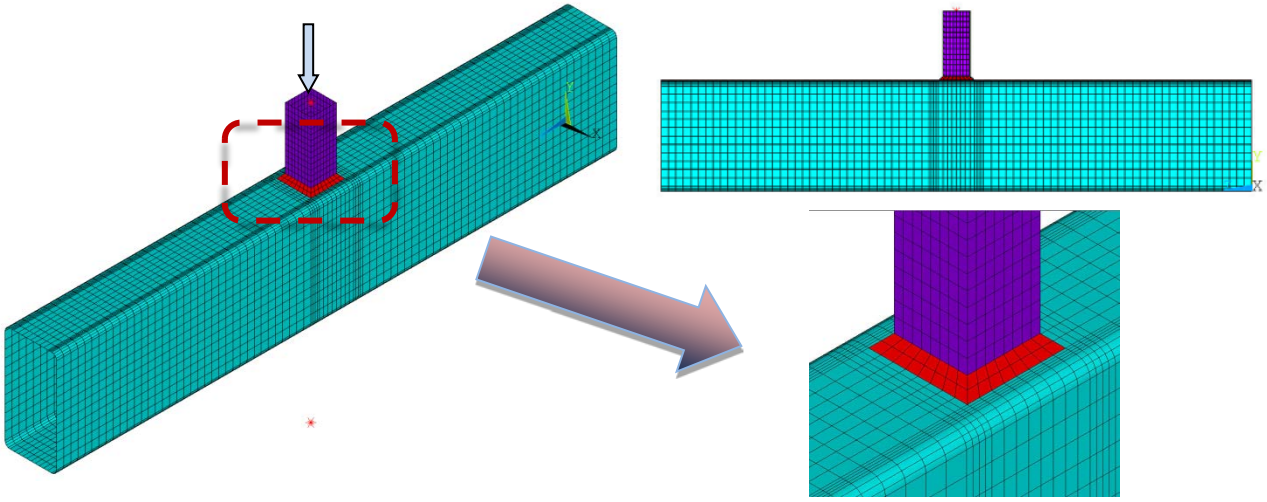

b) RHS tubular duplex stainless steel joints

Figure 4 – Finite element models

Table 1 – Material properties of duplex stainless steel tubes (in MPa)

Section (h x b x t)	E	σ_p	$\sigma_{0.1}$	$\sigma_y = \sigma_{0.2}$	$\sigma_{0.5}$	$\sigma_{1.0}$	σ_u	ε_f (%)
Chord 160x80x3	208000	167	481	536	570	595	766	40
Brace 40x40x2	216000	164	633	707	748	780	827	29

5 Numerical Model Calibration

In order to validate the numerical model developed in this work to evaluate the RHS stainless, the deformation limit criteria presented previously was applied. Additionally the verification made in terms of resistance of the studied joint, and corresponded to one of the joints tested experimentally by Feng and Young [10]. In this work the RHS tubular joint was made of a 160x80x2,96 chord and one 40x40x1,96 brace whose mechanical properties were presented in Tab. 1. In this test assumed a compressive axial load on the brace while the chord base was considered fully pinned in the rigid support of the test equipment. The load versus displacement curves used to compare the numerical and experimental results were obtained in a point distant 20mm from the brace edge. The numerical and experimental curves are presented in the Figure 5. Observing these curves, a reasonable agreement was verified and enable the development of a parametrical analysis for this joint type.

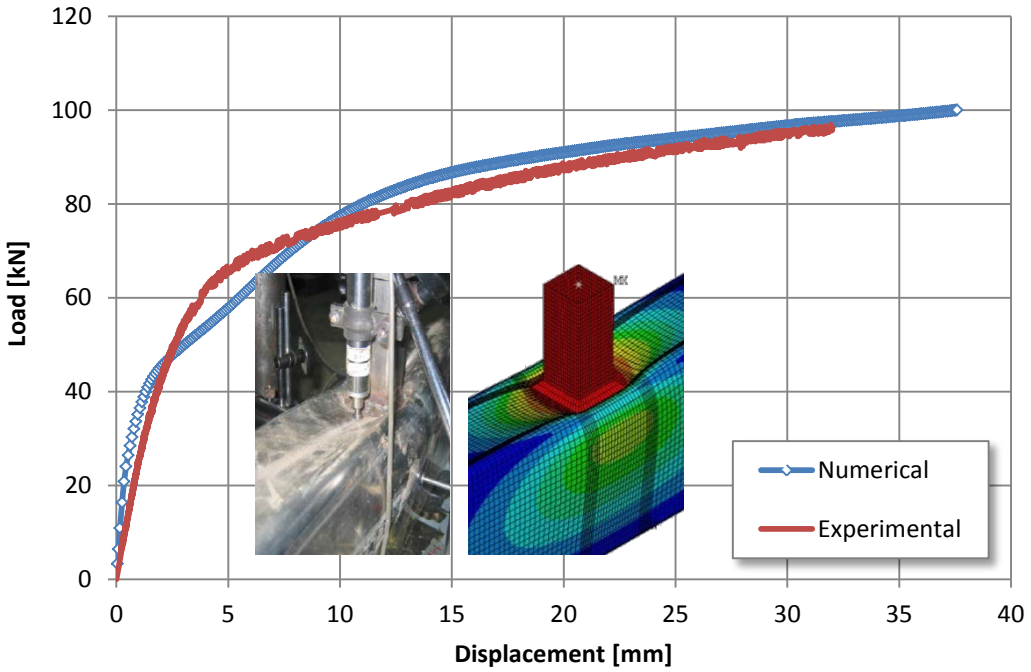

Figure 5 – Numerical versus experimental curves – RHS duplex stainless steel tubular joints

Due to the lack of test data a numerical calibration for the duplex stainless steel beams models was not performed. But it is necessary to observe that a similar model was calibrated and used to evaluate the structural response of carbon steel lateral torsional buckling beams.

6 Parametrical Analysis

6.1 Duplex stainless steel beams - LTB

In order to evaluate the lateral buckling capacity of duplex stainless steel beams, it was chosen adopted W300x150 welded profile had a 300mm height, 160mm flange width, 9.5mm flange thickness and 4.7mm web thickness. For this profile, eight span lengths were investigated, i.e., from 1 to 8m corresponding to values of λ_{LT} between 0.57 and 3.15. As mentioned before, an initial imperfection was applied in the model in order to evaluate the global response of the models and the lateral torsional buckling ultimate limit state. Figure 6 presents the numerical and analytical curves for these analysis where it can be observed that the Eurocode 3 equations related to the lateral torsional buckling ultimate limit state for carbon steel beams can also be used for duplex stainless steel profiles.

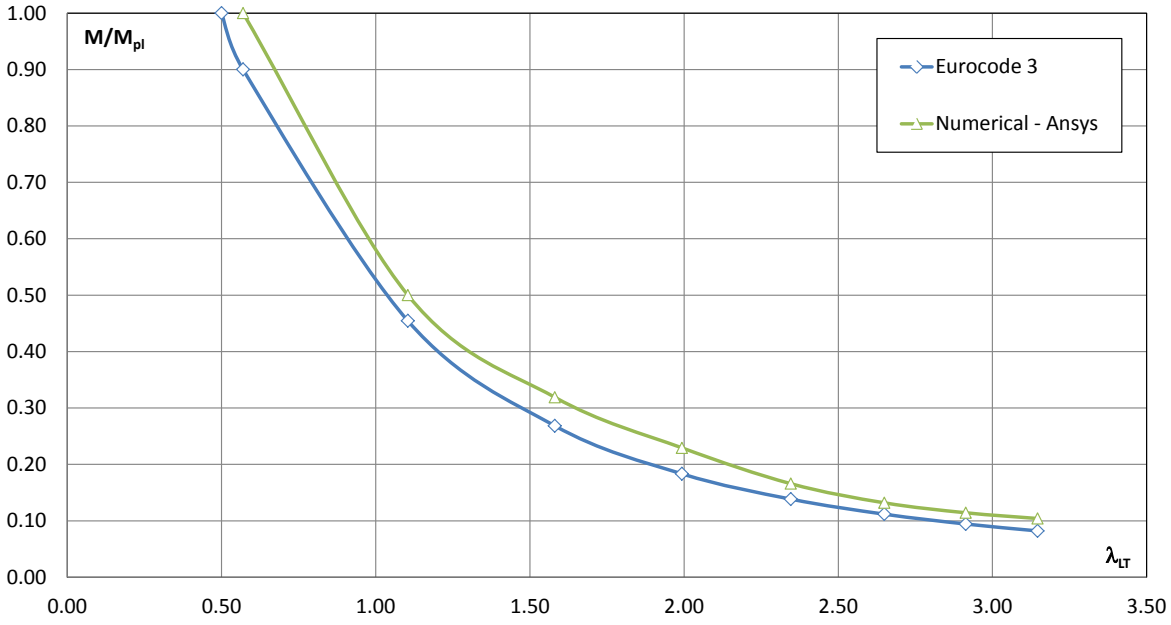

Figure 6 – Numerical versus Eurocode 3 –duplex stainless steel beams

With the aim of to show that the ultimate limit state that governs the beam design was lateral torsional buckling, the load versus displacement curve for the beam with 8m span with a concentrated load applied at midspan is presented in the Figure 7. In this curve, the ultimate bending moment was equal to 57.64 kN.m. For this load, the von Mises stress distribution is presented in the Figure 8 where it can be observed that the plastic bending moment resistance was not reached in this case, i.e., 479.61 kN.m. The used yield stress for the duplex stainless steel was equal to 526.68 MPa.

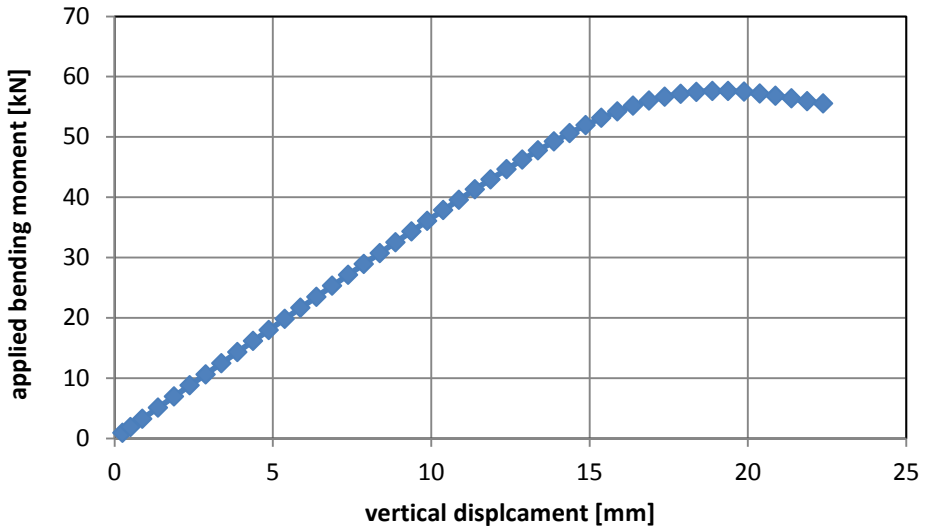

Figure 7 – Bending moment versus vertical displacement for duplex stainless steel beams

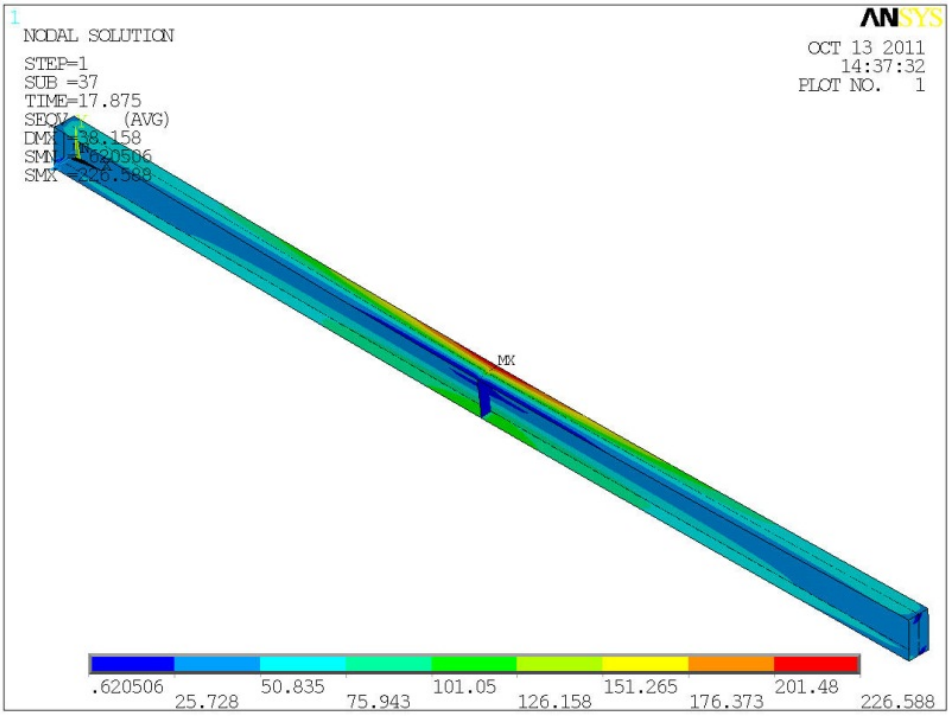

Figure 8 – Von Mises stress distribution - duplex stainless steel beams

6.2 RHS duplex stainless steel joints

In order to evaluate the resistance of tubular T joints between RHS members constituted by duplex stainless steel, ten models were considered according to Table 2. These models were chosen varying β value between 0.27 and 0.50. The comparison results were performed in terms of the resistances obtained from Eurocode 3, New CIDECT and Feng and Young formulation. At this point is important to emphasize that the two first codes are specific to carbon steel tubular joints. The last code introduced a modification in order to provide provisions for duplex stainless steel RHS tubular joints.

Table 2 – Geometrical characteristics for RHS duplex stainless steel joints

Model ID	Geometry							
	Chord			Brace			β	2γ
	h_0	b_0	t_0	h_1	b_1	t_1		
1	160.5	80.6	2.96	40.1	40.3	1.96	0.50	27.23
2	160.5	80.6	3.26	40.1	40.3	1.96	0.50	24.72
3	160.5	100.6	2.96	40.1	40.3	1.96	0.40	33.99
4	160.5	100.6	3.26	40.1	40.3	1.96	0.40	30.86
5	160.5	120.6	2.96	40.1	40.3	1.96	0.33	40.74
6	160.5	120.6	3.26	40.1	40.3	1.96	0.33	36.99
7	160.5	140.6	2.96	40.1	40.3	1.96	0.29	47.50
8	160.5	140.6	3.26	40.1	40.3	1.96	0.29	43.13
9	160.5	150.6	2.96	40.1	40.3	1.96	0.27	50.88
10	160.5	150.6	3.26	40.1	40.3	1.96	0.27	46.20

Table 3 – Comparison of results - RHS duplex stainless steel joints

Model ID	N_u	N_s	N_u/N_s	N_{def}	$N_{1,Rd}$	N_1^*	N_{1np}	$\frac{N_{1,Rd}}{N_{def}}$	$\frac{N_1^*}{N_{def}}$	$\frac{N_{1np}}{N_{def}}$
1	47.4	32.4	1.5	47.4	35.6	32.3	28.7	0.8	0.7	0.6
2	59.1	41.0	1.4	59.1	43.1	39.2	36.1	0.7	0.7	0.6
3	30.7	18.1	1.7	27.1	30.2	27.5	22.2	1.1	1.0	0.8
4	38.0	22.9	1.7	34.4	36.6	33.3	28.1	1.1	1.0	0.8
5	23.3	12.2	1.9	18.2	27.5	24.9	18.1	1.5	1.4	1.0
6	29.2	15.6	1.9	23.4	33.3	30.3	23.3	1.4	1.3	1.0
7	19.5	8.8	2.2	13.3	25.7	23.4	15.0	1.9	1.8	1.1
8	24.4	11.5	2.1	17.3	31.2	28.4	19.7	1.8	1.6	1.1
9	18.2	7.7	2.3	11.6	25.1	22.8	13.7	2.2	2.0	1.2
10	22.7	10.1	2.2	15.2	30.4	27.7	18.2	2.0	1.8	1.2

Observing Table 3, the new CIDECT formulation provides a better approximation to the numerical results when compared with Eurocode 3 results. But when these two values are compared with the Feng and Young values corresponding to N_{1np}/N_{def} in the Table 3, it may be concluded that this latter formulation presented better results when compared with the two first ones.

7 Conclusions

The present paper presented an investigation aiming to evaluate the lateral buckling capacity of duplex stainless steel beams and the resistance of tubular T joints between RHS members constituted by duplex stainless steel. The results were discussed and compared in terms of the stress distribution, force-displacement curves, etc.

The numerical results indicated that for the duplex stainless steel beams, the formulation presented in Eurocode 3 for carbon steel beams may be used for the case where duplex stainless steel beams. As for the duplex stainless steel tubular joints, the Feng and Youbg formulation presented better results when compared to the Eurocode 3 and CIDECT provisions.

Acknowledgments

The authors gratefully acknowledge the Brazilian National and State Science Support Agencies: CAPES, CNPq and FAPERJ for the financial support granted to this research program. Thank are also due to LABCIV - Civil Engineering Computer Laboratory, Faculty of Engineering, UERJ for the computational support.

References

[1] Gardner, L., Nethercot, D. A., Experiments on stainless steel hollow sections — Part 1: Material and cross-sectional behaviour. Journal of Constructional Steel Research, vol. 60, n.9, p. 1291–1318, 2004.

[2] Eurocode 3, ENV 1993-1-4, 2003: Design of steel structures – Part 1.4: General rules – Supplementary rules for stainless steel, CEN, European Committee for Standardisation, 2003.

[3] Eurocode 3, ENV 1993-1-1, 2003: Design of steel structures - Structures – Part 1-1: General rules and rules for buildings. CEN, European Committee for Standardisation, 2003.

[4] Silva, L. S. da, Simões, R., Gervásio, H., Design os Steel Structures, ECCS Eurocode Design Manuals, Ernest&Sohn, 2010.

[5] Packer, J.A., Wardenier, J., Zhao, X.-L., G.J. van der Vegte and Y. Kurobane. Design Guide - For Rectangular Hollow Section (RHS) Joints Under Predominantly Static Loading. CIDECT, 2009.

[6] Ansys 12.0 ®, ANSYS - Inc. Theory Reference, 2010.

[7] Cao, J.J. , Packer, J.A., Young, G.J. (1998). Yield line analysis of RHS connections with axial loads. Journal Constructional Steel Research. vol. 48, nº 1, pp 1-25.

[8] Choo, Y. S., Qian, X. D., Liew, J. Y. R, Wardenier, J. (2003). Static strength of thick-walled CHS Xjoints - Part I. New approach in strength definition. Journal of Constructional Steel Research. vol.59, pp. 1201-1228.

[9] Eurocode 3, ENV 1993-1-1, (2003). Design of steel structures - Structures - Part 1-1: General rules and rules for buildings. CEN. European Committee for Standardisation, Brussels, 2003.

[10] Feng, R., Young, B. (2008). Experimental investigation of cold-formed stainless steel tubular T-joints. Thin-Walled Structures, vol. 46, pp 1129-1142.

[11] Feng, R., Young, B. (2011). Design of cold-formed stainless steel tubular T- and X- joints. Journal of Constructional Steel Research vol. 67, pp 421-436.

[12] Kosteski, N., Packer, J.A., Puthli, R.S. (2003). A finite element method based yield load determination procedure for hollow structural section connections. Journal Constructional Steel Research. vol. 59, nº 4, pp. 427-559.

[13] Lee, M.M.K. (1999). "Strength, stress and fracture analyses of offshore tubular joints using finite elements". Journal of Constructional Steel Research. vol. 51, pp 265-286.

[14] Lu, L.H., de Winkel, G.D., Yu, Y., Wardenier, J. (1994). Yield line analysis of RHS connections with axial loads. Journal Constructional Steel Research. vol. 48, nº 1, pp 1-25.

[15] Lu, L.H., de Winkel, G.D., Yu, Y., Wardenier, J. (1994). Deformation limit for the ultimate strength of hollow section joints 6th International Symposium on Tubular Structures, Melbourne, Australia.

[16] Packer, J.A.(1993a). Moment Connections between Rectangular Hollow Sections. Journal Constructional Steel Research 25, pp 63-81.

[17] Packer, J.A., Wardenier, J., Kurobane, Y., Dutta, D., Yeomans, N.(1993b). Assemblages de sections creusesrectangulaires sous chargementstatique predominant. Série CIDECT "Construire avec des profiles creux", Verlag TUV Rheinland, Koln.

[18] Packer, J.A., Wardenier, J., Zhao, X.-L., G.J. van der Vegte and Y. Kurobane.(1993b). Design Guide - For Rectangular Hollow Section (RHS) Joints Under Predominantly Static Loading. CIDECT, 2009.

[19] Zhao, X.(2000). Deformation limit and ultimate strength of welded T-joints in cold-formed RHS sections. Journal of Constructional Steel Research, vol. 53, pp 149-165.